Available online at www.sciencedirect.com

ScienceDirect

Ceramics International 37 (2011) 1055–1061

CERAMICS INTERNATIONAL

www.elsevier.com/locate/ceramint

Facile synthesis of boron carbide elongated nanostructures via a simple in situ thermal evaporation process

Mohammad Jazirehpour *, Hamid-Reza Bahahrvandi, Ali Alizadeh, Naser Ehsani

Materials Science and Engineering Department, MUT University of Technology, Tehran 84817-75631, Iran

Received 2 August 2010; received in revised form 20 August 2010; accepted 14 November 2010
Available online 6 January 2011

Abstract

Boron carbide elongated nanostructures such as nanowires, nanobelts and nanosheets have been synthesized via a low-cost and simple in situ thermal evaporation process using commercially available B_4C powders as the main precursor. Heat treatments were done in the temperature range of 1400–1600 °C in the presence of Co nanoparticles (and $NiCl_2$ in some experiments) as the catalyst material. The growth mechanism of the nanostructures was proposed to be a cooperative growth procedure including surface diffusion, vapor–liquid–solid (VLS) and solid–liquid–solid (SLS) growth mechanisms. The final product, containing some of the initial B_4C particles and as-synthesized elongated nanostructures may be potentially applicable as an excellent reinforcing phase in composite materials. Moreover, nanostructures with right angle junctions were obtained from the sidewalls of the graphite boats, which may be operative in MEMS and NEMS devices. The samples have been characterized by scanning electron microscopy, transmission electron microscopy, X-ray diffraction and photoluminescence spectroscopy.

Keywords: Synthesis; Elongated nanostructures; Thermal evaporation; Boron carbide

1. Introduction

Boron carbide is a refractory p-type semiconductor with outstanding properties such as small thermal extension coefficient, high melting point, high hardness, low density, high corrosion and oxidation resistance, high neutron absorption cross section, excellent high temperature thermoelectric characteristics and good field emission properties [1–5]. Also, it has potential applications as ceramic armor for extreme conditions, reinforcement phase in composite materials, nozzles, bearings, dies and cutting tools, neutron absorbers, solid-state neutron detectors, high-temperature thermoelectric energy conversion and field emission devices [5–7].

Previously, boron carbide elongated nanostructures have been synthesized via different methods such as plasma enhanced chemical vapor deposition using orthocarborane as the source compound [8], electrostatic spinning and pyrolysis of a polymeric ceramic precursor (poly-norbornenyldecaborane) [9], carbon nanotube template based method in which boron carbide nanorods are directly prepared from the reaction between carbon nanotubes and boron powder [10,11], melt infiltration or vacuum filtration of polyhexenyldecaborane through porous anodized aluminum oxide (AAO) followed by pyrolysis and dissolution of the AAO in HF acid which yields boron carbide nanostructures [12], catalyst assisted carbothermal reduction of B_2O_3 [13], and catalyst free method via thermal evaporation of $B/B_2O_3/C$ powder precursor under argon atmosphere without the presence of catalyst [14].

These methods each have some shortcomings as well as advantages. Some methods such as the catalyst unassisted thermal evaporation and PECVD result in high quality nanostructures but in them the yield of products is low and large-scale synthesis may be expensive. Some others such as AAO templating, carbon nanotube template based and electrostatic spinning use rare expensive starting materials. Carbothermal reduction of boron oxide in the presence of catalyst metallic particles is a low-cost method but the products yielded thereof contain a significant amount of remained carbon; the elimination of the excess carbon is not easy.

The above-mentioned methods may be very suitable for some particular applications [5], but when the application of

* Corresponding author. Tel.: +98 31252206806; fax: +98 31252206806.
E-mail address: Jazirehpour@nano-ac.ir (M. Jazirehpour).

0272-8842/$36.00
doi:10.1016/j.ceramint.2010.11.028

boron carbide nanostructures is intended as a reinforcing phase, purification dispensability and chemical homogeneity of reinforcing particles besides low-cost and facile large-scale synthesis capability become the most important factors. In this case, the excellent quality of nanostructures and morphological homogeneity are depressed to next precedence. Therefore, developing a method with large-scale and low-cost synthesizing capability is still needed.

The aim of this research is the synthesis of a reinforcing mixture containing boron carbide nanostructures in a large scale via a facile and low-cost method. The mentioned mixture is expected to have an enhanced reinforcing capability due to elongated shapes of the nanostructures [15,16]. However, in the present method, for kinetic reasons, the starting powder is not completely converted to the mentioned nanostructures and initial B_4C powders are somewhat remained in the final product but this morphological inhomogeneity is not disadvantageous at all [16–18] because the starting powders have also reinforcing effects; besides boron carbide particles are currently used as a reinforcing phase in different composite materials [19–21]. It is well known that elongated nanostructures (such as nanowires, nanorods and nanobelts) have enhanced reinforcing effects due to both nanosize effects and morphological characteristics [15,22,23]. The final product, which contains boron carbide initial powders accompanied by nanowires, nanobelts and nanosheets, might exhibit an improved reinforcing effect due to the presence of elongated nanostructures [16,24–26].

2. Experimental procedure

Commercially available B_4C powder (99.7%, AEE) and cobalt nanoparticles (28 nm, IoLiTec) were separately suspended in ethanol. The cobalt nanoparticle suspension was sonicated for 1 h before its addition to B_4C/ethanol suspension, NaCl was added to the mixture as the vaporizer. The suspension was heated and vigorously stirred on a magnetic stirrer to remove ethanol. Finally dried powder containing the basic molar ratios $B_4C_P:Co_{np}:NaCl = 1:0.02:0.1$ was placed in a graphite boat. The boat was then placed at the center of a tube furnace. Other examinations were done with $B_4C_P:Co_{np}$ molar ratios of 1:0.05 and 1:0.1. Also the effect of more vaporization agents was investigated by the examination of a starting mixture containing $B_4C_P:Co_{np}:NaCl = 1:0.02:0.5$. Argon gas (>99.9%) was introduced with a rate of 200 standard cubic centimeters per minute and the boat was heated up and kept at the maximum set temperatures (1400–1600 °C in different examinations) for 2 h. Some other examinations were done and B_4C powders were mixed with $NiCl_2$ as a catalyst source. A molar ratio of $B_4C:NiCl_2 = 1:0.1$ was used; other conditions were repeated without any change.

Scanning electron microscopy (SEM, LEO 1450VP), transmission electron microscopy (TEM, Philips EM208) and X-ray diffraction (XRD, Seifert XRD 3003TT, Cu Kα radiation, $\lambda = 0.154$ nm) were employed to characterize the as-received samples. Photoluminescence (PL) spectroscopy of nanostructures was carried out by a HITACHI F-4500 spectroscopy system using a 530 nm excitation light at room temperature.

3. Results and discussion

Fig. 1 shows the typical XRD pattern of the samples after heat treatment at 1600 °C for 2 h. The pattern can be indexed to rhombohedral B_4C crystal (the JCPDS card 35-0798).

Various morphologies of the as-synthesized nanostructures in the sample, which contains cobalt nanoparticles as the catalyst material at 1600 °C for 2 h, are shown in Fig. 2(a). Nanowires and nanobelts could be easily recognized in the SEM image. In Fig. 2(a) some larger elongated nanostructures are signed with arrows. Generally, the diameters of the nanowires are in the range of 30–150 nm, although the nanobelts have widths of about 0.3–2 μm and thicknesses in the range of 50–150 nm. TEM image of a typical nanowire and its higher magnification have been presented in Fig. 2(b) and (c). Striations along the nanowire are revealing a twined structure. Formation of twins in low temperature synthesized boron carbide has been confirmed and discussed previously [27,28]. A belt-like nanostructure with smooth surface and uniform width is shown in Fig. 2(d). Striations across the nanobelt in Fig. 2(d) are observable as the ripple-like vibrations during TEM investigation; nanostructures during the growth process may encounter various stresses, which may result in bending and some remnant strains in their crystal lattice. The mentioned phenomenon during TEM investigation may be due to interactions between electron beams and wried atomic layers at the surface of the nanobelts. Without using NaCl as the vaporizer, no nanostructures were formed and this shows the presence of vaporization agents (here, chlorine containing compounds) is a key feature in the current process. Also using the starting mixture of $B_4C_P:Co_{np}:NaCl = 1:0.02:0.5$ with more NaCl, the results showed no significant improvement and the total amount of the synthesized nanostructures was reduced. Only few sparse nanowires were observed in the as synthesized sample with starting mixture of $B_4C_P:Co_{np}:NaCl = 1:0.02:0.5$.

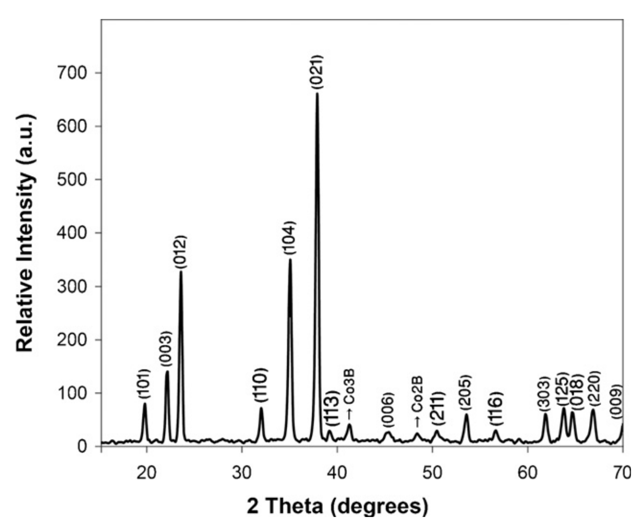

Fig. 1. The typical XRD pattern of the samples after heat treatment at 1600 °C for 2 h.

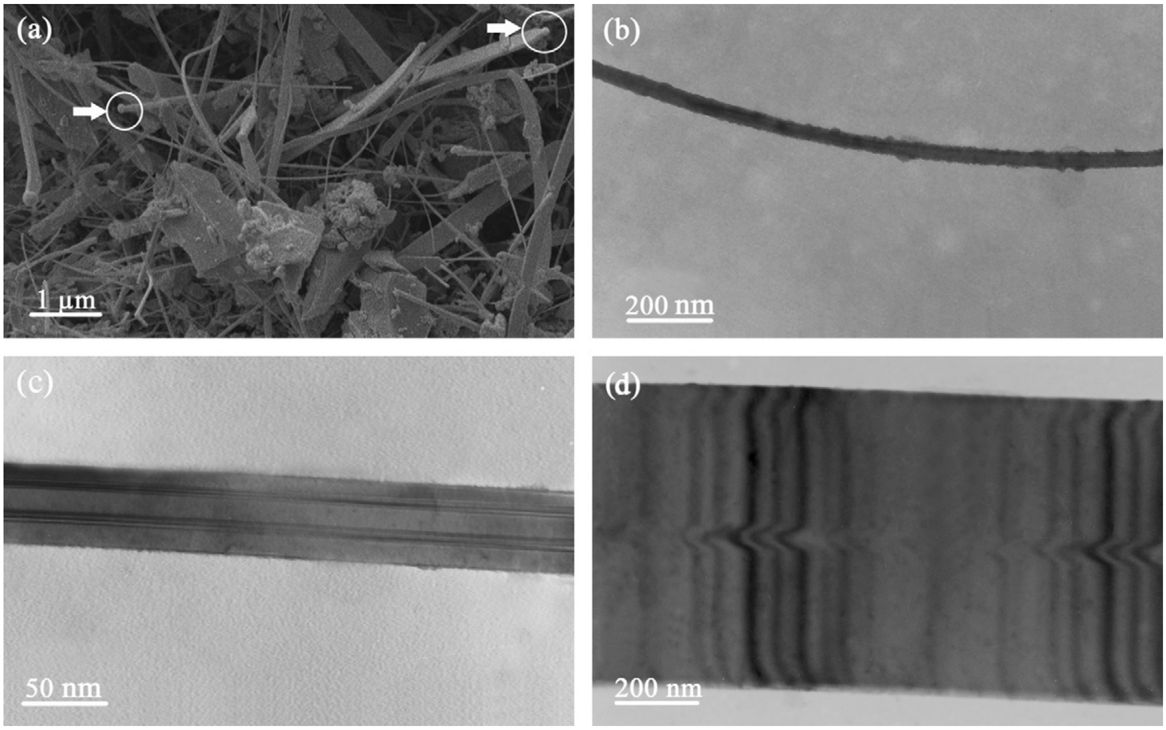

Fig. 2. (a) Various morphologies of nanostructures in the sample, which contained cobalt nanoparticles and heat-treated at 1600 °C for 2 h, (b) TEM image of a typical nanowire, (c) TEM image of a nanowire with higher magnification which reveals its twined structure, and (d) TEM image of a typical nanobelt.

The reason may be the rapid exhaustion of the catalyst material as a result of the applying of additional vaporizing agent; the increase of argon feeding rate (1000 sccm) led to a similar result.

Further examinations were done to investigate the effect of different amounts of catalyst material. Additional amounts of catalyst material resulted in the formation of coarse whiskers with several-micron thicknesses. This further amount of the catalyst material results in larger catalyst droplets which consequently lead to the formation of larger structures [29].

As mentioned in Section 2, the synthesis process was done in different temperatures in the range of 1400–1600 °C in different examinations. The melting point of the catalyst metal (Co) is 1495 °C and according to nanosize effect, the melting point of nanoparticles could be reduced several degrees [8]. Nevertheless, the amount of nanostructures in the synthesis products was negligible when the synthesis temperature was below 1500 °C and the best results were gained at 1600 °C. Additional keeping time at the synthesis temperature had no

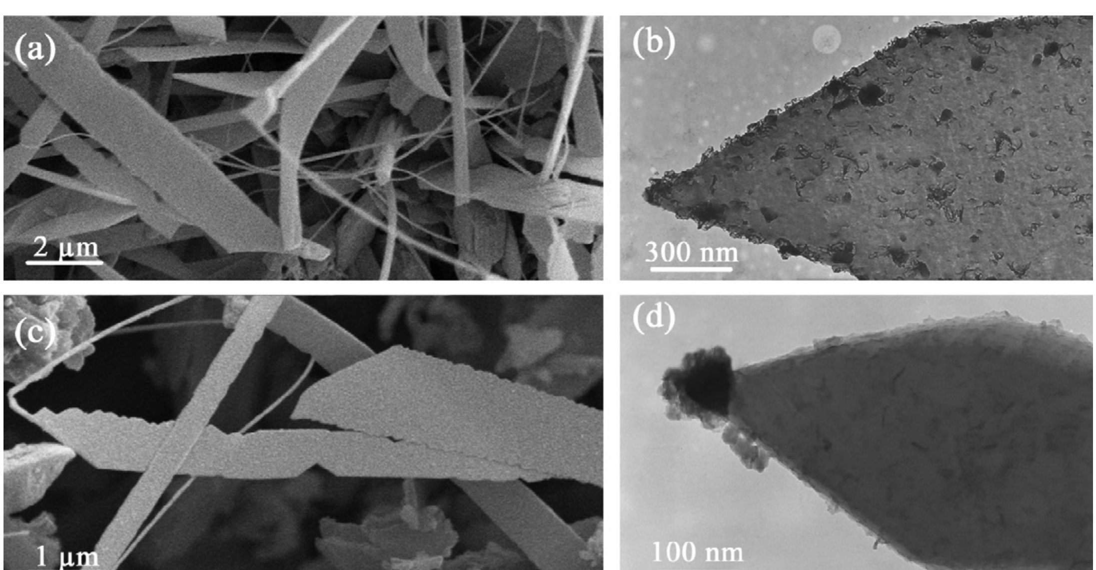

Fig. 3. (a) Nanosheets, nanobelts and nanowires in the sample, which contained $NiCl_2$ and heat-treated at 1600 °C for 2 h, (b) TEM image of a typical nanosheet with rough surface, (c) SEM image of saw-toothed nanosheets, and (d) TEM image of a pencil-like nanostructure with a catalyst particle at its tip.

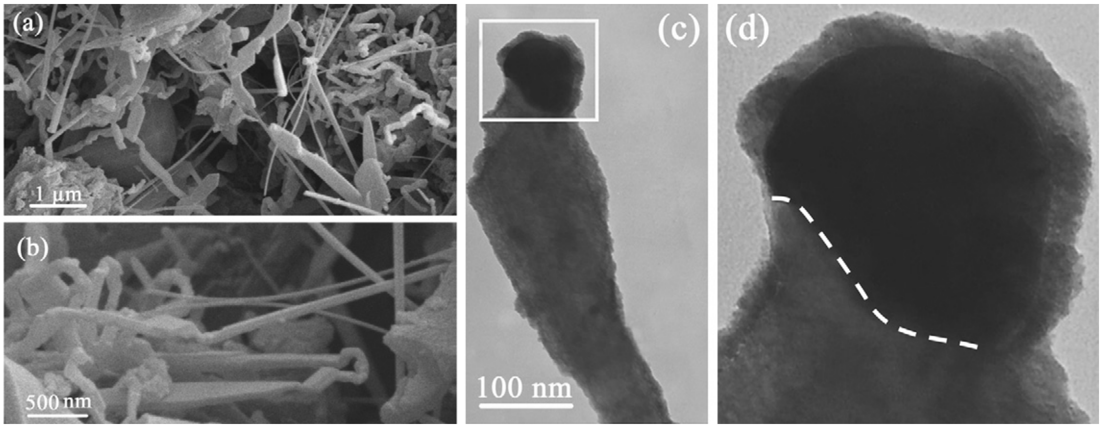

Fig. 4. (a) Nanowires and wired nanostructures in the sample, which contained $NiCl_2$ and heat-treated at 1400 °C for 2 h, (b) higher magnification image from wired nanostructures, (c) TEM image of a wired nanostructure with a catalyst particle at its tip, and (d) higher magnification image from the catalyst–nanostructure interface.

significant effect on raising the amount of nanostructures. It seems that due gradual exhaustion of vaporization agent as well as the catalyst material during the synthesis process, no improvement could be achieved with further increasing the time.

The effect of the $NiCl_2$ as a catalyst material was also investigated. The SEM image of nanostructures, which have been synthesized after the heat treatment of the $NiCl_2$ added sample at 1600 °C for 2 h, is shown in Fig. 3(a) in which various morphologies such as nanowires, nanobelts and nanosheets are observable. According to Fig. 3(c) some nanosheets have saw-toothed edges; the formation of the saw-toothed edges is usually ascribed to the presence of stacking faults between the teeth and the nanosheet [30]. Samples were further characterized by transmission electron microscopy; a higher magnification image from the surface of a typical nanosheet and a pencil-like nanostructure with a catalyst droplet at its tip are exhibited in Fig. 3(b) and (d). The surfaces of the nanosheets are somedeal rough; it may arise from temperature reduction at the end of the heat treatment time. Temperature reduction results in condensation and precipitation of boron carbide constituent vapors when the furnace is turned off. Therefore, some of the preformed nanostructures may also act as more preferred sites for precipitation of these vapors.

$NiCl_2$ added sample, which is heat-treated at 1400 °C for 2 h (Fig. 4(a) and (b)), obviously contains nanowires and wried nanostructures; wryness of the nanostructures may result from nanoscale local temperature and gas flow fluctuations [31]. Mentioned fluctuations can change the preferred growth direction and result in the wried shapes [32,33].

Fig. 4(c) and (d) illustrates a typical wried nanostructure with a catalyst droplet at its tip, the higher magnification TEM

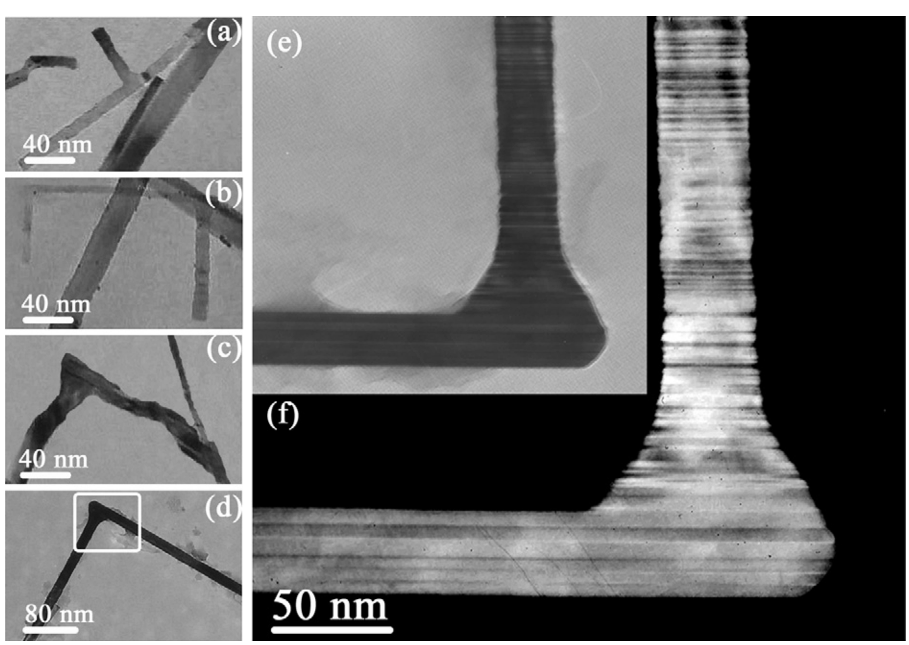

Fig. 5. (a–d) Nanostructures with right angle junctions, (e) higher magnification image from the L-shaped nanostructure in (d), (f) the same image in (e) with enhanced contrast.

image of the catalyst droplet shows the interface between the catalyst droplet and the nanostructure is a curved line. A dashed line in Fig. 4(d) signs the interface. The uneven interfaces are very important for nanostructures growth, because the atomic steps are easily generated at the bottom of such interfaces. In the uneven interfaces, there is often more than one low-energy liquid–solid interface during the growth of crystals and this is the source of uneven interfaces [34,35].

It was probable that the location of the product also play a role in the final product, when the walls of the graphite boats were scratched and further characterized by transmission electron microscopy; nanostructures with right angle junctions were observed. Such nanostructures with right angle junctions are exhibited in Fig. 5(a)–(f). A higher magnification TEM image from Fig. 5(d) is shown in Fig. 5(e) with enhanced image contrast, where the structure of the nanostructure is more clearly visible. The L-shaped nanostructure contains striations in its structure, which could be attributed to stacking faults or twins. An interesting phenomenon is observable in the junction point: striations along the horizontal branch in the junction point extend across the vertical one and create an L-shaped junction. Right angle junctions may be formed due to nanoscale local temperature and gas flow fluctuations that could change the preferred growth direction. Previously, the effects of the temperature on the growth direction of nanostructures have been investigated [35,36].

Since visible optical applications for L-shaped nanostructures were not unthinkable, photoluminescence properties of these nanostructures were studied. The room temperature photoluminescence spectrum of the nanostructures with right angle junctions under a 530 nm light excitation source is observable in Fig. 6. The spectrum exhibits a broad PL emission centered at 620 nm. Previously, photoluminescence properties of bulk boron carbide have been investigated and the center of PL emission has been observed at 1.563 eV (792 nm) [37]. The mentioned observations have been attributed to the indirect allowed recombination of free excitons [37,38]. In addition, electron–phonon interactions or distributions of different energy levels of trap centers may be conceivable in the formation of the broad PL emission. Considering the PL emission of bulk boron carbide in comparison with that of

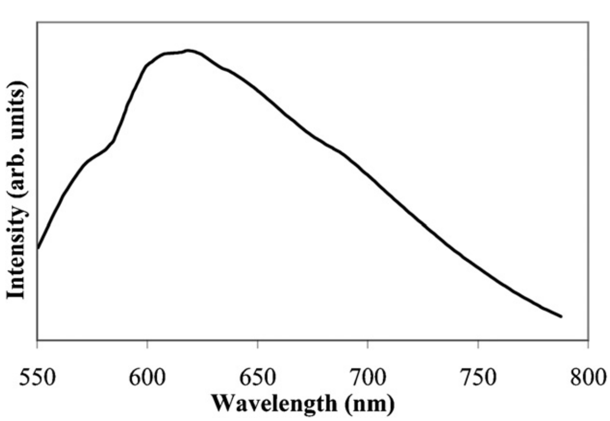

Fig. 6. The typical photoluminescence spectrum of boron carbide nanostructures.

boron carbide nanostructures with right angle junctions, one can observe a blue shift, which could be indexed to quantum size effect [39,40]. According to PL emission spectrum of boron carbide nanostructures with right angle junctions, visible optical applications for these nanostructures may be supposable.

According to the applied synthesis process and because of using catalyst materials both vapor–liquid–solid (VLS) [41,42] and solid–liquid–solid (SLS) [43] mechanisms may be probable. In well known VLS mechanism, the catalyst material, firstly, creates melted alloy droplets and catalyst droplets adsorb feedstock vapors from the surrounding space; when droplets become supersaturated, the growth of nanowires (or whiskers) through the liquid droplets are started (Fig. 7(a)). Comparative evaporation of boron carbide ingredients takes place at the maximum set temperature in the presence of NaCl as a volatilizing agent. The generated vapors may directly react to form solid B_4C or adsorb in catalyst droplets and act via VLS mechanism. Besides VLS mechanism, SLS mechanism is also supposed to be operative. In SLS mechanism, the molten catalyst combined with B_4C to form a liquid droplet containing boron and carbon. Boron and carbon may be introduced into the molten catalyst from direct solution of B_4C at the interface of initial B_4C particle and catalyst droplet or surface diffusion of ingredients; finally coexisting B and C in the molten catalyst droplet precipitate and crystallize as elongated nanostructures (Fig. 7(b)). Reactions in VLS and SLS mechanisms are listed below (some reactions are not equilibrated).

Reactions via VLS mechanism:

$$NaCl_{(L)} \rightarrow NaCl_{(g)} \rightarrow Na_{(g)} + Cl_{(g)} \quad (1)$$

$$B_4C_{(s,\,powder)} + Cl_{(g)} \rightarrow 4BCl_{(g)} + C \quad (2)$$

$$Co_{(L)} + C_{(s)} \rightarrow Co{-}C_{(L)} \quad (3)$$

$$Co{-}C_{(L)} + BCl_{(g)} \rightarrow Co{-}C{-}B_{(L)} + CoCl_{2(g)} \quad (4)$$

$$Co{-}C{-}B_{(L)} \rightarrow B_4C_{(s,\,elongated\ nanostructures)} + Co_{(L)} \quad (5)$$

Reactions via SLS mechanism:

$$B_4C_{(s,\,powder)} + Co_{(L)} \rightarrow Co{-}C{-}B_{(L)} \rightarrow B_4C_{(s,\,elongated\ nanostructures)} + Co_{(L)} \quad (6)$$

The functions of VLS and SLS mechanisms in growth of nanowires and nanobelts are demonstrated by schematic models in Fig. 7. Regardless the general similarities in the growth process of nanobelts and nanowires, it seems that the formation of the nanobelts and the other elongated platelets, which have smaller thicknesses and larger widths, could not be explained only via VLS and SLS mechanisms. Therefore, the growth of the nanobelts may be initiated by VLS and SLS mechanisms and subsequently their specific shapes be guided by surface diffusion of constituent species. According to the proposed formation mechanism (Fig. 7), this is the random distribution of catalyst particles that is dictating which type of elongated nanostructures (nanowires or nanobelts) can form; where the catalyst particles are distributed sporadically,

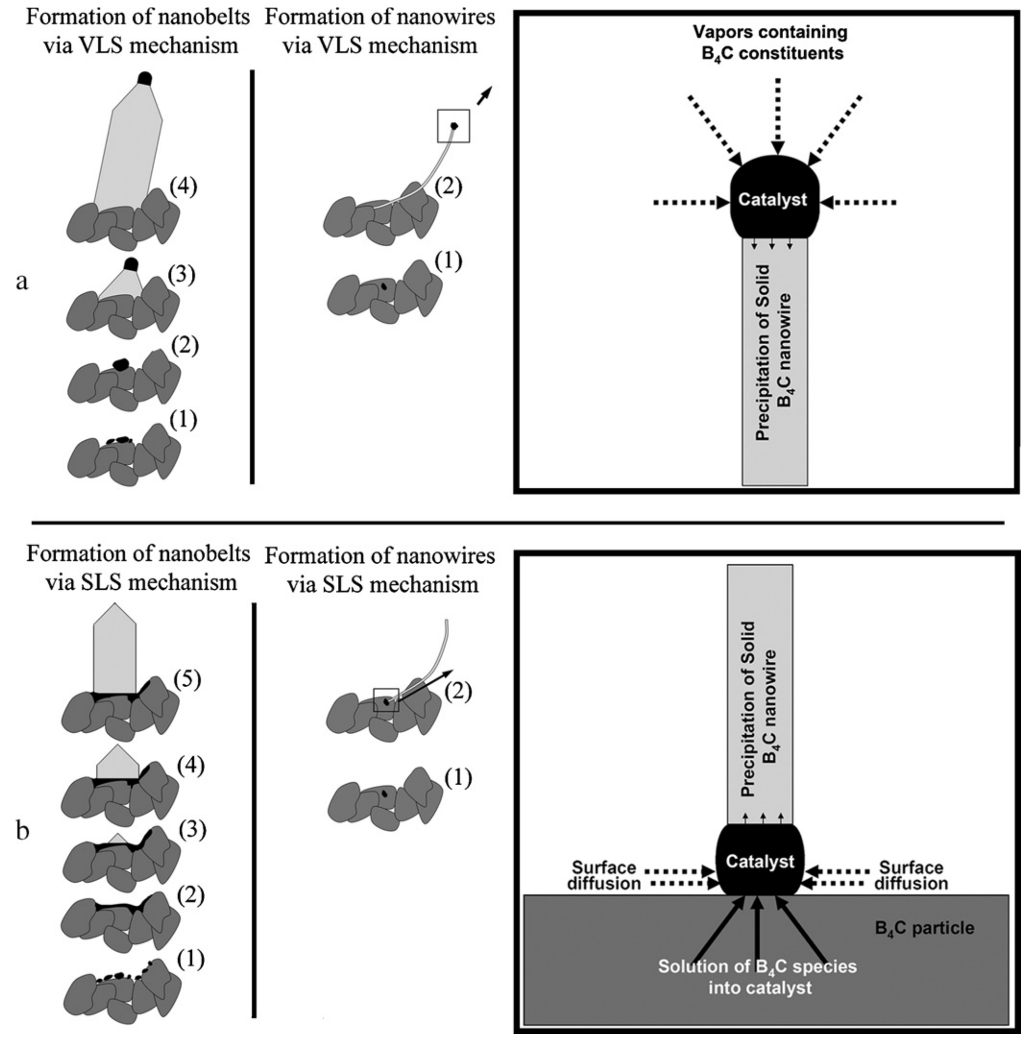

Fig. 7. (a) The growth of nanowires and nanobelts via VLS mechanism, (b) the growth of nanowires and nanobelts via SLS mechanism. Big squares in the right column of (a) and (b) are magnified view of the small squares in the middle column of (a) and (b). Small black dots in the small squares and gray lines in the middle column of (a) and (b) represent catalyst nanoparticles and nanowires, respectively.

formation of nanowires is more probable but where the distribution of catalyst nanoparticles is in a manner that conditions are prone to the formation of a melted catalyst layer or a larger catalyst droplet on the powder substrate, therefore, production of the belt-like structures is more probable.

4. Conclusion

A facile low-cost method is presented with large scale production capability of a reinforcing mixture containing boron carbide nanostructures such as nanowires, nanobelts and nanosheets via a catalyst-assisted thermal evaporation process in the presence of chlorine containing compounds (such as NaCl) as a volatilizing agent which is one of the most key features in the current process. In addition, $NiCl_2$ was used as a multipurpose material, which acts as the vaporizing agent, as well as the catalyst material. Both VLS and SLS mechanisms may act in the formation of the nanostructures and the functions of these mechanisms were described by schematic models. In addition, nanostructures with right angle junctions were obtained from the walls of the graphite boats and characterized by transmission electron microscopy; these nanostructures may be applicable in MEMS applications. Subsequently, photoluminescence properties of nanostructures were characterized and a broad PL emission centered at 620 nm was observed, which revealed a blue shift in comparison with that of bulk boron carbide. Altogether, the final products, containing initial B_4C particles and as-synthesized nanostructures, may be potentially applicable as the reinforcing phase in composite materials but further investigations are needed to exactly evaluate the reinforcing effects of such nanostructures in practical applications.

References

[1] C. Wood, D. Emin, Conduction mechanism in boron carbide, Physical Review B 29 (8) (1984) 4582–4587.
[2] F. Thévenot, Boron carbide—a comprehensive review, Journal of the European Ceramic Society 6 (4) (1990) 205–225.
[3] R. Lazzari, N. Vast, J.M. Besson, S. Baroni, A. Dal Corso, Atomic structure and vibrational properties of icosahedral B4C boron carbide, Physical Review Letters 83 (16) (1999) 3230–3233.

[4] A.O. Sezer, J.I. Brand, Chemical vapor deposition of boron carbide, Materials Science and Engineering B: Solid State Materials for Advanced Technology 79 (3) (2001) 191–202.

[5] L.H. Bao, C. Li, Y. Tian, J.F. Tian, C. Hui, X.J. Wang, C.M. Shen, H.J. Gao, Single crystalline boron carbide nanobelts: synthesis and characterization, Chinese Physics B 17 (11) (2008) 4247–4252.

[6] M.W. Chen, J.W. McCauley, K.J. Hemker, Shock-induced localized amorphization in boron carbide, Science 299 (5612) (2003) 1563–1566.

[7] D. Emin, T.L. Aselage, A proposed boron-carbide-based solid-state neutron detector, Journal of Applied Physics 97 (1) (2005) 013529.

[8] D.N. McIlroy, A. Alkhateeb, D. Zhang, D.E. Aston, A.C. Marcy, M.G. Norton, Nanospring formation—unexpected catalyst mediated growth, Journal of Physics-Condensed Matter 16 (12) (2004) R415–R440.

[9] D.T. Welna, J.D. Bender, X.L. Wei, L.G. Sneddon, H.R. Allcock, Preparation of boron-carbide/carbon nanofibers from a poly(norbornenyldecaborane) single-source precursor via electrostatic spinning, Advanced Materials 17 (7) (2005) 859–862.

[10] W.Q. Han, P. Kohler-Redlich, F. Ernst, M. Ruhle, Formation of (BN)(x)C-y and BN nanotubes filled with boron carbide nanowires, Chemistry of Materials 11 (12) (1999) 3620–3623.

[11] J.Q. Wei, B. Jiang, Y.H. Li, C.L. Xu, D.H. Wu, B.Q. Wei, Straight boron carbide nanorods prepared from carbon nanotubes, Journal of Materials Chemistry 12 (10) (2002) 3121–3124.

[12] M.J. Pender, L.G. Sneddon, An efficient template synthesis of aligned boron carbide nanofibers using a single-source molecular precursor, Chemistry of Materials 12 (2) (2000) 280–283.

[13] M. Carlsson, F.J. Garcia-Garcia, M. Johnsson, Synthesis and characterisation of boron carbide whiskers and thin elongated platelets, Journal of Crystal Growth 236 (1–3) (2002) 466–476.

[14] R.Z. Ma, Y. Bando, High purity single crystalline boron carbide nanowires, Chemical Physics Letters 364 (3–4) (2002) 314–317.

[15] V. Valcarcel, A. Perez, M. Cyrklaff, F. Guitian, Novel ribbon-shaped alpha-Al_2O_3 fibers, Advanced Materials 10 (16) (1998) 1370–1373.

[16] H.L. Liu, C.Z. Huang, X.Y. Teng, H. Wang, Effect of special microstructure on the mechanical properties of nanocomposite, Materials Science and Engineering A: Structural Materials Properties Microstructure and Processing 487 (1–2) (2008) 258–263.

[17] Y.Y. Li, J.Z. Cui, The multi-scale computational method for the mechanics parameters of the materials with random distribution of multi-scale grains, Composites Science and Technology 65 (9) (2005) 1447–1458.

[18] H.L. Liu, C.Z. Huang, J. Wang, B.Q. Liu, Study on the multi-scale nanocomposite ceramic tool material, Advances in Machining & Manufacturing Technology Viii 315–316 (2006) 118–122.

[19] I. Kerti, F. Toptan, Microstructural variations in cast B4C-reinforced aluminium matrix composites (AMCs), Materials Letters 62 (8–9) (2008) 1215–1218.

[20] R.M. Mohanty, K. Balasubramanian, S.K. Seshadri, Boron carbide-reinforced alumnium 1100 matrix composites: fabrication and properties, Materials Science and Engineering A: Structural Materials Properties Microstructure and Processing 498 (1–2) (2008) 42–52.

[21] J. Onoro, M.D. Salvador, L.E.G. Cambronero, High-temperature mechanical properties of aluminium alloys reinforced with boron carbide particles, Materials Science and Engineering A: Structural Materials Properties Microstructure and Processing 499 (1–2) (2009) 421–426.

[22] W. Nhuapeng, W. Thamjaree, S. Kumfu, P. Singjai, T. Tunkasiri, Fabrication and mechanical properties of silicon carbide nanowires/epoxy resin composites, Current Applied Physics 8 (3–4) (2008) 295–299.

[23] B. Fiedler, F.H. Gojny, M.H.G. Wichmann, M.C.M. Nolte, K. Schulte, Fundamental aspects of nano-reinforced composites, Composites Science and Technology 66 (16) (2006) 3115–3125.

[24] M.H.G. Wichmann, K. Schulte, H.D. Wagner, On nanocomposite toughness, Composites Science and Technology 68 (1) (2008) 329–331.

[25] S.R.C. Vivekchand, U. Ramamurty, C.N.R. Rao, Mechanical properties of inorganic nanowire reinforced polymer–matrix composites, Nanotechnology 17 (11) (2006) S344–S350.

[26] E.T. Thostenson, C.Y. Li, T.W. Chou, Nanocomposites in context, Composites Science and Technology 65 (2005) 491–516.

[27] S. Prochazka, S.L. Dole, C.I. Hejna, Abnormal grain growth and microcracking in boron carbide, Journal of the American Ceramic Society 68 (9) (1985) C235–C236.

[28] G.I. Kalandadze, S.O. Shalamberidze, A.B. Peikrishvili, Sintering of boron and boron carbide, Journal of Solid State Chemistry 154 (1) (2000) 194–198.

[29] R. Ma, Y. Bando, Investigation on the growth of boron carbide nanowires, Chemistry of Materials 14 (10) (2002) 4403–4407.

[30] C. Ma, D. Moore, J. Li, Z.L. Wang, Nanobelts, nanocombs, and nanowindmills of wurtzite ZnS, Advanced Materials 15 (3) (2003) 228–231.

[31] M. Jazirehpour, A. Alizadeh, Synthesis of boron carbide core–shell nanorods and a qualitative model to explain formation of rough shell nanorods, Journal of Physical Chemistry C 113 (5) (2009) 1657–1661.

[32] Y. Lilach, J.P. Zhang, M. Moskovits, A. Kolmakov, Encoding morphology in oxide nanostructures during their growth, Nano Letters 5 (10) (2005) 2019–2022.

[33] B. Wang, Y.H. Yang, C.X. Wang, G.W. Yang, Growth and photoluminescence of SnO_2 nanostructures synthesized by Au–Ag alloying catalyst assisted carbothermal evaporation, Chemical Physics Letters 407 (4–6) (2005) 347–353.

[34] S.K. Lok, G. Wang, Y. Cai, N. Wang, Y.C. Zhong, K.S. Wong, I.K. Sou, Growth temperature dependence of the structural and photoluminescence properties of MBE-grown ZnS nanowires, Journal of Crystal Growth 311 (9) (2009) 2630–2634.

[35] N. Wang, Y. Cai, R.Q. Zhang, Growth of nanowires, Materials Science & Engineering R-Reports 60 (1–6) (2008) 1–51.

[36] Y. Cai, S.K. Chan, I.K. Sou, Y.T. Chan, D.S. Su, N. Wang, Temperature-dependent growth direction of ultrathin ZnSe nanowires, Small 3 (1) (2007) 111–115.

[37] R. Schmechel, H. Werheit, T.U. Kampen, W. Monch, Photoluminescence of boron carbide, Journal of Solid State Chemistry 177 (2) (2004) 566–568.

[38] N. Vast, S. Baroni, G. Zerah, J.M. Besson, A. Polian, M. Grimsditch, J.C. Chervin, Lattice dynamics of icosahedral alpha-boron under pressure, Physical Review Letters 78 (4) (1997) 693–696.

[39] A.I. Ekimov, F. Hache, M.C. Schanneklein, D. Ricard, C. Flytzanis, I.A. Kudryavtsev, T.V. Yazeva, A.V. Rodina, A.L. Efros, Absorption, Intensity-dependent photoluminescence measurements on CdSe quantum dots: assignment of the first electronic transitions, Journal of the Optical Society of America B: Optical Physics 10 (1) (1993) 100–107.

[40] D. Nesheva, C. Raptis, Z. Levi, Resonant Raman scattering and photoluminescence in SiO_x/CdSe multiple quantum wells, Physical Review B 58 (12) (1998) 7913–7920.

[41] R.S. Wagner, W.C. Ellis, Vapor–liquid–solid mechanism of single crystal growth, Applied Physics Letters 4 (5) (1964) 89–90.

[42] A.M. Morales, C.M. Lieber, A laser ablation method for the synthesis of crystalline semiconductor nanowires, Science 279 (5348) (1998) 208–211.

[43] K.W. Kolasinski, Catalytic growth of nanowires: vapor–liquid–solid, vapor-solid-solid, solution-liquid–solid and solid–liquid–solid growth, Current Opinion in Solid State & Materials Science 10 (3–4) (2006) 182–191.